applied sciences

MDPI

Article

Application and Validation of a Simplified Approach to Evaluate the Seismic Performances of Steel MR-Frames

Rosario Montuori [1], Elide Nastri [2], Vincenzo Piluso [2], Alessandro Pisapia [2] and Paolo Todisco [2,*]

[1] Department of Pharmacy, University of Salerno, 84084 Fisciano, Italy; r.montuori@unisa.it
[2] Department of Civil Engineering, University of Salerno, 84084 Fisciano, Italy; enastri@unisa.it (E.N.); v.piluso@unisa.it (V.P.); alpisapia@unisa.it (A.P.)
* Correspondence: ptodisco@unisa.it

Abstract: The main aim of this work is to validate the application of a simplified performance-based method for assessing the seismic performance of steel buildings, focusing particularly on Moment Resisting Frames (MRFs) through nonlinear analyses. This simplified method defines the capacity curve of a structure through elastic and rigid-plastic analyses, calibrated by regression analyses conducted on 420 structures. To assess its accuracy, the method was compared with other analytical approaches, including incremental dynamic analyses (IDA) provided by existing codes. These analyses were performed on both real structures and simulated designs, considering recent and older codes. The comparison of capacity results derived from code-based approaches and IDA, aligned with the limit states outlined in current codes, showcased the high reliability of the proposed simplified assessment approach.

Keywords: moment resisting frames; structural capacity; performance-based assessment; simplified methods; IDA analysis

Citation: Montuori, R.; Nastri, E.; Piluso, V.; Pisapia, A.; Todisco, P. Application and Validation of a Simplified Approach to Evaluate the Seismic Performances of Steel MR-Frames. *Appl. Sci.* **2024**, *14*, 1037. https://doi.org/10.3390/app14031037

Academic Editor: Marek Krawczuk

Received: 5 December 2023
Revised: 22 January 2024
Accepted: 23 January 2024
Published: 25 January 2024

1. Introduction

In order to prevent significant structural damage by guaranteeing adequate ductility and energy dissipation capacity, Mazzolani and Piluso [1] proposed the well-known design methodology called "Theory of Plastic Mechanism Control (TPMC)" in 1997. The original version of this method is based on the extension of the kinematic theorem of plastic collapse to the concept of mechanism equilibrium curve, and, recently, a closed-form solution has been developed and applied to different steel structural typologies [2,3]. This approach has been applied only to new buildings in order to avoid partial failure mechanisms, such as the well-known soft-storey mechanism, by ensuring the achievement of the global mechanism type under severe seismic actions. However, recently, a new performance design method, also based on the TPMC approach, has been developed to evaluate the behaviour of the existing buildings. In fact, the assessment of the seismic vulnerability of existing structures has become, in recent years, a topic of increasing importance among those developed by structural engineering [4–11]. Infrastructures, but also simple buildings, need to be checked and verified against seismic loading to design any intervention in seismic enhancement or retrofitting. The planning of seismic risk mitigation has shown that it is of fundamental importance to carry out a rapid classification of the existing building heritage in terms of seismic performance [12–18].

The performance of a building is evaluated by comparing its ability to dissipate incoming seismic energy due to structural ductility and seismic demand. If the demand for ductility is lower than the capacity, the structure, even if damaged, does not collapse, ensuring, in this case, the primary requirement of performance from the point of view of the Ultimate Limit States (ULS), namely the protection of human lives. Otherwise, i.e., when the demand for ductility is higher than the capacity, the structure collapses because it is not able to dissipate the incoming seismic energy satisfactorily and, therefore, to develop an

adequate collapse mechanism [19–21]. The main difficulties in creating a satisfactory model for the prediction of seismic damage concern the quantitative definition of the degree of damage corresponding to each expected performance level. The complete knowledge of the seismic performance of a structure is the result of sophisticated numerical procedures such as static or nonlinear dynamic analysis [22–26]. Such analyses require the structural model to be adequately accurate to capture nonlinear behaviour. However, especially for large-scale assessments and the planning of seismic risk mitigation interventions, a simplified methodology able to describe the capacity curve analytically and quickly without resorting to more complex analyses could be extremely useful, given a code implementation. As a result, a simplified methodology for different structural types has been developed to evaluate the capacity of an existing building without resorting to static or dynamic nonlinear analysis [27–30]. To calibrate this model, a wide parametric analysis was carried out on 420 frames designed according to three different approaches [27]. The non-dimensional pushover curve has been simplified by defining three branches: an elastic response branch, a plateau branch corresponding to the maximum bearing capacity, and a descending branch corresponding to the mechanism equilibrium curve. The result is a simplified trilinear model. In addition, this model allows the definition of four characteristic points (A, B, C, D) corresponding to specific performance levels, associated with the limit states provided by the existing codes. ("Fully Operational" (FO), "Operational" (O), "Life Safety" (LS), "Near Collapse" (NC)).

This paper validates the proposed method by applying it to 420 steel MRFs designed using three distinct approaches. A pushover analysis is conducted for each MRF, and the obtained results are compared with those obtained from the simplified method. Additionally, the methodology is employed in two case studies involving simulated designs based on outdated code provisions. The accuracy of the proposed method is evaluated through incremental dynamic analyses (IDA) performed on a collection of seven recorded accelerograms using the OpenSees computer program. Furthermore, the results in terms of spectral acceleration coming from the IDA analyses have been compared with those provided by the application of the proposed assessment procedure and the current European code provisions.

2. Simplified Trilinear Non-Dimensional Pushover Curve

In this section, the simplified performance-based methodology defined and calibrated in [25] is reported as the basis of the work herein presented. In particular, the fundamental equations of the model are summarised and, consequently, validated through pushover analyses.

2.1. Theory Remarks

The simplified performance-based methodology herein investigated is based on a simplified trilinear non-dimensional pushover curve, derived as the envelope of three branches [27]: (1) elastic branch; (2) maximum bearing capacity branch, obtained through the calibrated Merchant-Rankine formula; and (3) mechanism equilibrium curve.

The user can reproduce a pushover or a non-dimensional pushover curve, as depicted in Figure 1, with target points identified through mathematical relationships. The identification of the most-prone collapse mechanism can be attained through rigid-plastic analysis. By considering column sections and the distribution of static forces, this method yields the determination of the first-order collapse multipliers α_0 and, regarding the second-order effects, the slopes γ_s of the collapse mechanism equilibrium curve for each type of potential collapse mechanism [19,27] (Figure 2). The mechanism that will be more prone to develop is the one corresponding to the curve characterised by the lower values of α, in the range of displacements compatible with the local ductility resources.

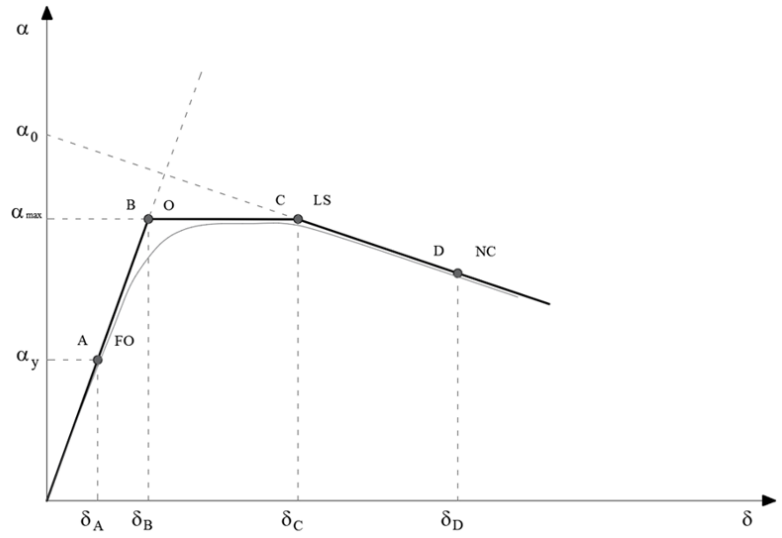

Figure 1. Trilinear approximation of the non-dimensional pushover curve.

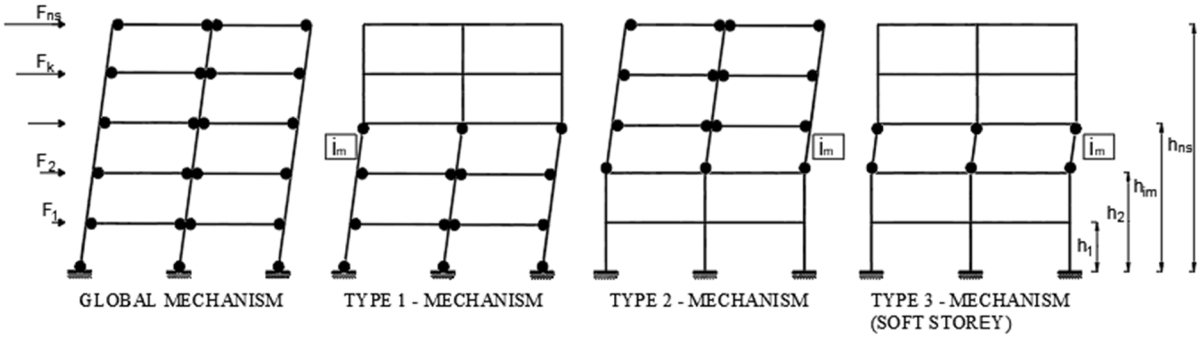

Figure 2. Collapse mechanism of MR-Frames.

Below are the main equations of the proposed model, whose complete discussion can be found in [25–29]. In Figure 1, the most prone collapse mechanisms affecting seismic-resistant structures are reported.

The equations of the three branches in the $\alpha - \delta$ plane (horizontal force multiplier—top sway displacement) are as follows:

$$Elastic\ branch\ \rightarrow \alpha = \frac{1}{\delta_1}\delta \tag{1}$$

where δ_1 is the top sway displacement corresponding to the design horizontal forces. The horizontal branch can be expressed by the following:

$$Horizontal\ branch\ \rightarrow \alpha = \alpha_{max} = \frac{\alpha_0}{1 + \Psi\alpha_0\gamma_s\delta_1} \tag{2}$$

where:

$$\Psi = a + b\xi \qquad \xi = \sum \frac{EI_b}{L_b} / \sum \frac{EI_c}{L_c} \tag{3}$$

E is Young's modulus, I_b and I_c are the inertia moduli of the beams and columns, respectively, while L_b and L_c represent the lengths of the beams and columns, respectively. For the coefficient Ψ, the following relation is provided:

$$\Psi = 0.28488 - 0.14042\xi \tag{4}$$

Finally, in accordance with the rigid-plastic analysis, the final branch is given by the following:

$$Softening\ branch\ \rightarrow \alpha = \alpha_0 - \gamma_s(\delta - \delta_y) \tag{5}$$

where δ_y is the top sway displacement corresponding to the formation of the first plastic hinge.

The specific performance points (A, B, C, D, see Figure 1) associated with pre-defined limit states [30], identifying a target performance level, can be derived as follows:

- Point A—Fully Operational :

$$\alpha_A = \frac{1}{\delta_1}\delta_A \tag{6}$$

where δ_A is the displacement corresponding to the minimum between the displacement in the service conditions, and the formation of the first plastic hinge.

- Point B—Operational :

$$\alpha_B = \alpha_{max} \qquad \delta_B = \alpha_{max}\delta_y \tag{7}$$

where α_{max} is the maximum multiplier [25].

- Point C—Life Safety :

$$\alpha_C = \alpha_{max} \qquad \delta_C = \delta_{mecc} = \frac{\alpha_0 - \alpha_{max}}{\gamma_s} + \delta_y \tag{8}$$

- Point D—Near Collapse :

$$\alpha_D = \alpha_{max} - \gamma_s(\delta_D - \delta_C) \qquad \delta_D = \delta_C + \left(\vartheta_{p.u} - \vartheta_{p.mec}\right)H_0 \tag{9}$$

where $\vartheta_{p.u}$ is the plastic hinge rotation capacity, equal 8.0 ϑ_y according to EN 1988-1-3 [31], ϑ_y represents the chord rotation at yielding and it is defined with reference to the property of the members [25], H_0 is the collapse mechanism height. Finally, $\vartheta_{p.mec}$ is the plastic hinge rotation demand to attain the collapse mechanism.

An analytical formulation is reported for assessing plastic rotations in the critical structural elements [25]. This formulation is based on a "shear-type" single-storey portal with varying plastic moments at the column tops and bases. The derived relationships aim to estimate the plastic rotation demand associated with the formation of the collapse mechanism:

$$\frac{\vartheta_{p.mec}H_0}{n_s\delta_y} = \frac{\Psi_1}{\Psi_2}\Psi_3\left(\frac{\alpha_{max}}{\alpha_y} - 1\right)^{\Psi_4}\frac{1 - \Psi_5\gamma_s}{1 - \Psi_6\gamma_s} \tag{10}$$

and:

$$\frac{\vartheta_{p.mec}H_0}{n_s\delta_y} = \frac{\Psi'_1}{\Psi'_2}\Psi_3\left(\frac{\alpha_{max}}{\alpha_y} - 1\right)^{\Psi'_4}\frac{1 - \Psi'_5\gamma_s}{1 - \Psi'_6\gamma_s} \tag{11}$$

In particular, the coefficient with the apex refers to the element achieving the collapse (i.e., the critical element), with those without the apex to the element developing the first yield. The Ψ_i coefficients to be used in Equations (10) and (11), are given by the following relations:

$$\begin{array}{cc} \Psi_1 = a_1 + b_1 n_b & \Psi'_1 = a'_1 + b'_1 n_b \\ \Psi_2 = a_2 + b_2 n_s & \Psi'_2 = a'_2 + b'_2 n_s \\ \Psi i = a_i + b_i\xi \quad i = 3,\ldots,6 & \Psi' i = a'_i + b'_i\xi \quad i = 3,\ldots,6 \end{array} \tag{12}$$

where n_b is the number of bays, n_s is the number of storeys, while the coefficient ξ is defined in Equation (3). The values of the parameters a_i, b_i a'_i, b'_i are reported in [25] with reference to Global Moment Resisting Frames (GMRFs) designed according to TPMC,

Special Moment Resisting Frames (SMRFs) designed according to EN 1998-1-1 [32], and Ordinary Moment Resisting Frames (OMRFs) designed without any requirement aimed at the control of collapse mechanism.

2.2. Validation

A wide comparative analysis has been performed with reference to G-, S-, and O-Moment Resisting Frames. The analysis encompassed 140 distinct geometric configurations of low-rise frames. These variations involved adjusting the number of bays, n_b from 2 to 6, the number of storeys, n_s from 2 to 8, and the bay span at 3.00 m, 4.50 m, 6.00 m, and 7.50 m. Additionally, three different design approaches were considered for a total of 420 designed structures. All configurations were evaluated with dead loads (G_k) set at 3.50 kN/m^2, live loads (Q_k) at 3.00 kN/m^2 and an inter-storey height of 3.50 m [27].

Pushovers have been carried out using the SAP2000 computer program (v.24) [33] with a load pattern distribution compliant with the first vibration mode.

Beams (Figure 3) and columns (Figure 4) have been modelled as beam-column elements with plastic hinges ("P-hinge" elements) located at their ends. Plastic hinges accounting for the interaction between axial force and bending moment have been defined for columns, while for beams the axial force interaction has been neglected. The pushover analysis has been led under displacement control considering both geometrical and mechanical non-linearities.

Moment SF = M_{pl}		**Rotation SF = 1**
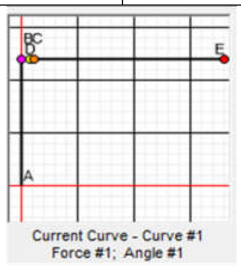		
Point	**Moment/yield Moment**	**Rotation/SF**
A	0	0
B	1	0
C	1	0.04
D	1	0.06
E	1	1

Figure 3. Moment/rotation model for beams.

P = P_y	**M_3 =M_{pl}**
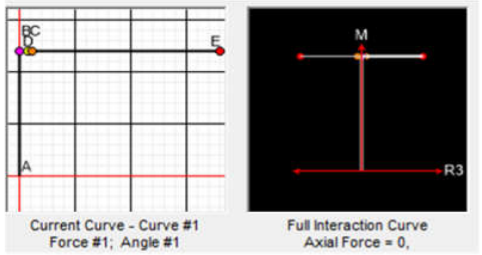	

Point	**Moment/yield Moment**	**Rotation/SF**
A	0	0
B	1	0
C	1	0.04
D	1	0.06
E	1	1

Figure 4. Moment/rotation model for columns.

The accuracy of the proposed trilinear model is depicted in Figures 5 and 6. In particular, a comparison between the results of the pushover analysis and those derived by the simplified approach is provided with reference to the prediction of displacements δ_c and δ_D. The x-axis denotes the theoretical values obtained by Equations (8) and (9), while the y-axis represents the values derived by SAP 2000.

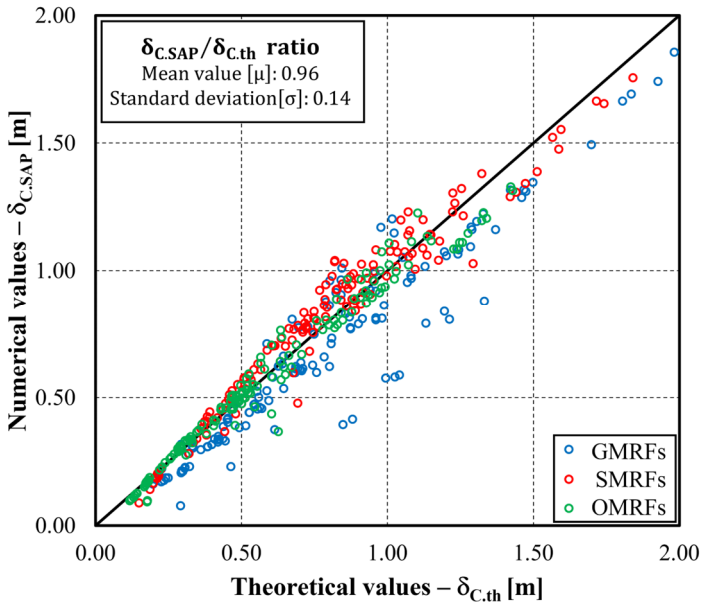

Figure 5. Accuracy of simplified approach in the prediction of δ_c.

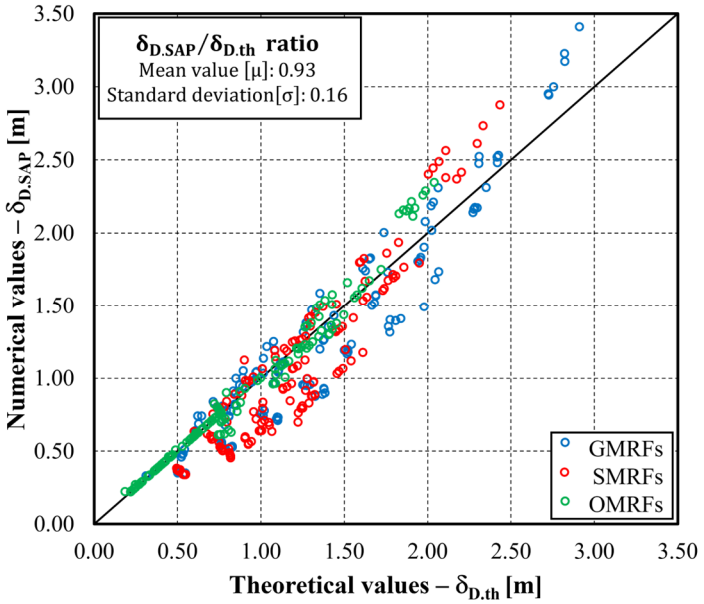

Figure 6. Accuracy of simplified approach in the prediction of δ_D.

By observing Figures 5 and 6, it is immediately evident that the accuracy of the simplified approach is very high. In fact, in the case of δ_c, the mean value of the ratio $\delta_{C.SAP}/\delta_{C.th}$ is 0.96 with a standard deviation equal to 0.14, while, in the prediction of δ_D, the mean value is about 0.93 with a standard deviation of 0.16.

3. Case Studies

In this section, two case studies have been analysed to evaluate the accuracy of the simplified approach with reference to the existing buildings.

The first building is a Moment Resisting Frame belonging to a five-storey building consisting of five symmetrical bays of 4.00 m in each direction. The building was designed according to a pre-1970 design code. The reference site has been hypothesised in L'Aquila (high seismic risk area in Italy $a_g/g = 0.261$ for a return period of 475 years), and it is characterised by a type B soil and a topographic category T1. The floors have been designed to withstand a variable load of 2.00 kN/m^2 and a permanent non-structural load of 2.00 kN/m^2. The inter-storey height is 3.00 m, the thickness of the floors is 140 mm, and the total height of the building is 15.00 m. The weight per unit volume of concrete is assumed to be 24.00 kN/m^3. The beams are IPE300 sections, while the columns are HEA400 sections, both of S355 ($f_y = 355$ MPa). Figure 7a depicts the planimetric configuration of the building and the tributary area of the analysed frame, while Figure 7b indicates the designed cross-sections and the seismic forces.

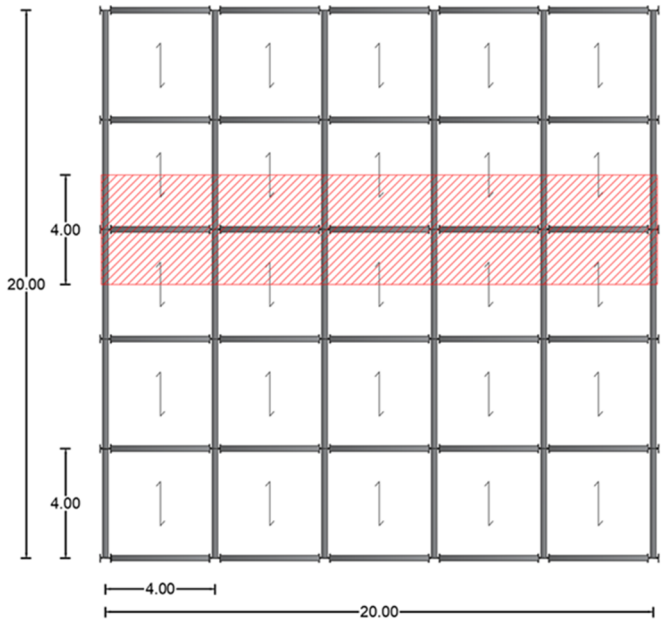

(**a**)

(**b**)

Figure 7. Plan configuration with tributary area (**a**); frontal view of the frame (**b**).

The second case study is an MR Frame belonging to a three-storey building, as reported in Figure 8, whose plan configuration is depicted in Figure 9a.

Figure 8. Pictures of the second case study.

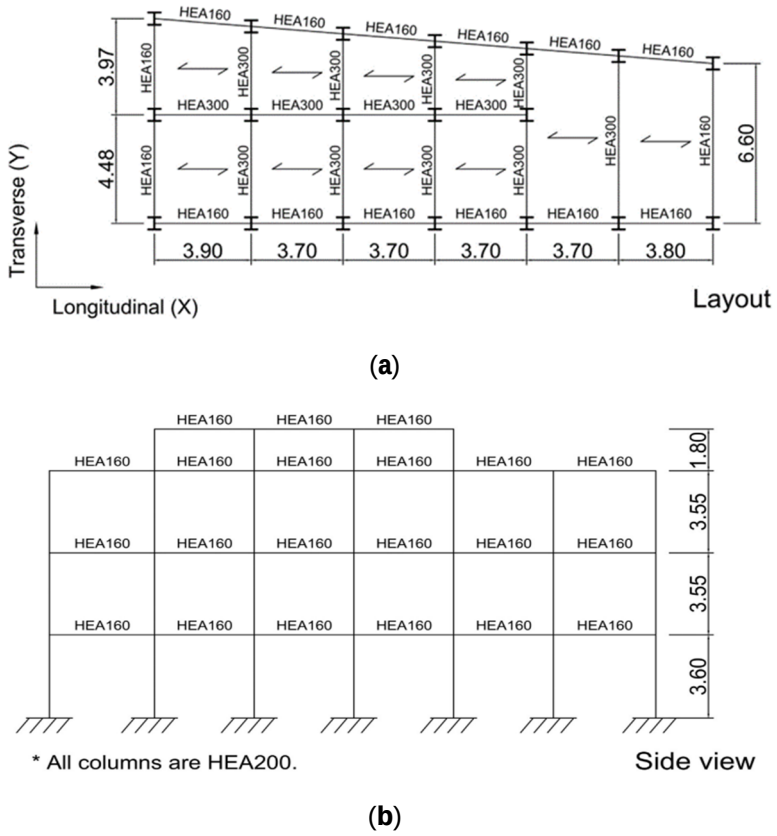

Figure 9. Plan configuration (**a**); Transversal section of the structure (**b**).

The building, located in Amatrice, Italy, was built some decades ago, before the introduction of modern seismic design standards. The building was damaged during the Central Italy earthquakes (24 August 2016 and 30 October 2016). The building lies on type B soil in the topographic category T1 [18]. The building plan is trapezoidal, measuring 6.60 m in the smaller front and 8.50 m in the larger one. It is approximately 22.5 m long. The inter-storey height is variable (about 3.60 m), as reported in Figure 10.

The floors have been designed to withstand a variable load of 2.00 kN/m^2 and a permanent non-structural load of 1.76 kN/m^2.

The flooring systems consist of concrete slabs on a corrugated sheet of steel with a thickness of 10 mm. The cross-sections of the outer and inner beams are HEA160 and HEA300, respectively, and all columns are HEA200 (Figure 9b).

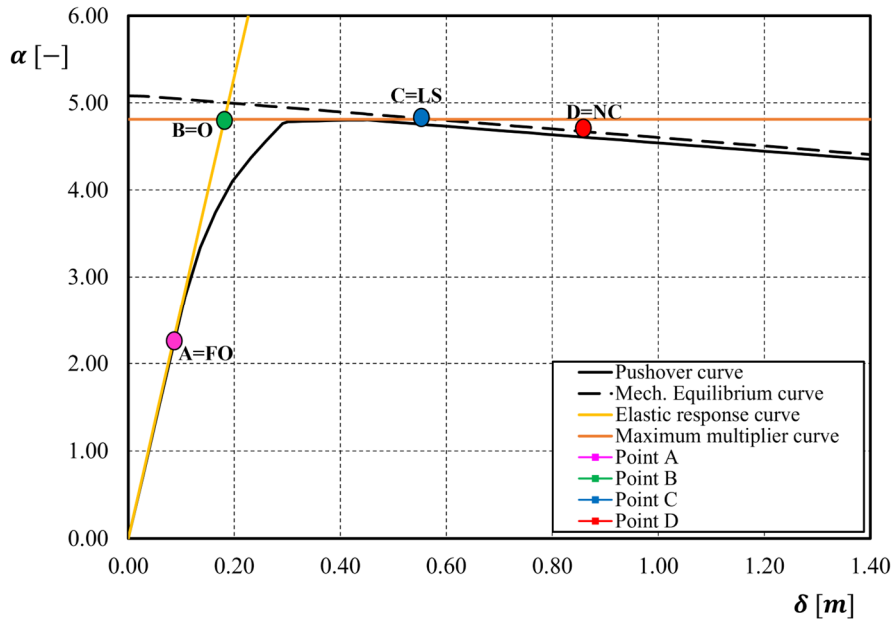

Figure 10. Comparison between the Pushover curve and those obtained by the trilinear model for case study 1.

4. Nonlinear Static Analysis

The collapse mechanism equilibrium curve [27] can be obtained by a rigid-plastic analysis extended to second-order effects.

First, it is necessary to evaluate, for each possible collapse mechanism, the first-order collapse multiplier α_0 and the corresponding slope of the mechanism equilibrium curve γ_s. The mechanism that will be activated in a field of displacements compatible with the local ductility supplies will be the one characterised by the equilibrium curve located below the others.

Tables 1 and 2 show the results of the first kinematic multiplier $\alpha_{0.im}^{(t)}$ and the slope of the equilibrium curve $\gamma_{im}^{(t)}$ for each failure mechanism according to the TPMC method [27–30] and for case 1 and 2, respectively. In particular, in case study 1, the collapse mechanism occurs according to the partial failure mechanism type-2, according to Figure 2, while the soft-storey mechanism, i.e., type-3 mechanism, occurs in case study 2.

Starting from the trilinear approximation of the push-over curve, the four characteristic points of the structural behaviour curve have been identified, and each of these points is associated with a specific limit state. They have been determined according to Equations (6)–(9), and their values are reported in Table 3 with reference to both case studies.

Table 1. First-order collapse multiplier and slopes of the mechanism equilibrium curves for case study 1.

Storey i_m	*Failure Mechanisms According to TPMC*					
	Type-1		**Type-2**		**Type-3**	
	$\alpha_{0.im}^{(1)}$ [-]	$\gamma_{im}^{(1)}$ [m^{-1}]	$\alpha_{0.im}^{(2)}$ [-]	$\gamma_{im}^{(2)}$ [m^{-1}]	$\alpha_{0.im}^{(3)}$ [-]	$\gamma_{im}^{(3)}$ [m^{-1}]
1	10.96	3.02	**5.04**	**0.49**	10.96	3.02
2	6.81	1.41	7.41	0.59	11.74	2.59
3	5.62	0.88	10.13	0.72	13.70	2.26
4	5.27	0.63	16.46	0.99	18.26	2.01
5	5.39	0.49	32.87	1.81	32.87	1.81

Table 2. First-order collapse multiplier and slopes of the mechanism equilibrium curves for the case study 2.

Storey i_m	*Failure Mechanisms According to TPMC*					
	Type-1		**Type-2**		**Type-3**	
	$\alpha_{0.im}^{(1)}$ [-]	$\gamma_{im}^{(1)}$ [m^{-1}]	$\alpha_{0.im}^{(2)}$ [-]	$\gamma_{im}^{(2)}$ [m^{-1}]	$\alpha_{0.im}^{(3)}$ [-]	$\gamma_{im}^{(3)}$ [m^{-1}]
1	0.66	1.64	1.17	0.48	**0.66**	**1.64**
2	1.27	0.77	1.80	0.61	0.96	1.43
3	1.33	0.48	3.00	1.07	1.58	1.07

Table 3. Values of α and δ according to the simplified approach.

Case Study	*Point A*		*Point B*		*Point C*		*Point D*	
	α_A [-]	δ_A [m]	α_B [-]	δ_B [m]	α_C [-]	δ_C [m]	α_D [-]	δ_D [m]
1	2.27	0.086	4.81	0.181	4.81	0.554	4.66	0.858
2	0.42	0.096	0.53	0.124	0.53	0.188	0.40	0.254

In order to evaluate the accuracy of the trilinear model obtained, a static nonlinear analysis, or push-over, was carried out using the SAP2000 computer program [33].

In Figures 10 and 11, the non-dimensional pushover curves obtained by SAP2000 are compared with those obtained by the trilinear model described in Section 3.

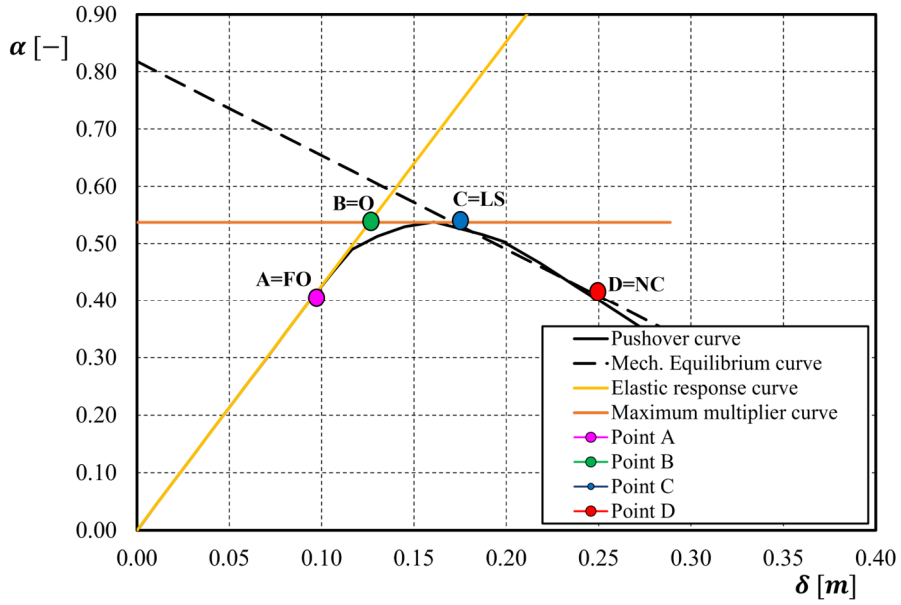

Figure 11. Comparison between Pushover curve and those obtained by the trilinear model for the case study 2.

5. Incremental Dynamic Analysis (IDA)

In order to evaluate the accuracy of the proposed method in the estimation of the spectral acceleration capacity for the presented case studies, a comparison with the results obtained by Incremental Dynamic Analyses has been reported.

5.1. Evaluation of the Capacity in Terms of Spectral Acceleration by Simplified Method

After defining the trilinear model and the performance points, the transformation procedure of the multiple degrees of freedom (MDOF) system into an equivalent single degree of freedom (SDOF) system was applied through the modal participation coefficient Γ.

Subsequently, the dynamic properties of the SDOF system, the simplified curve, and the performance points were represented in the ADRS plan. In this way, the capacity in terms of spectral displacements and accelerations was defined according to the "ADRS spectrum" and *Nassar and Krawinkler* models [34–36].

It was, therefore, necessary to define the nondimensional eigenvectors:

$$\underline{\Phi} = \{\phi_1, \phi_2, \phi_3, \phi_4, \phi_5\} \quad (\text{Case Study1}) \qquad \underline{\Phi} = \{\phi_1, \phi_2, \phi_3\} \quad (\text{Case Study2}) \tag{13}$$

where:

$$\phi_k = F_k / F_{n_s} \tag{14}$$

where F_k is equal to seismic force at $k-th$ storey and F_{n_s} is the seismic force at top storey according to EN 1998-1-1 [32]. The ϕ_i values are reported in Table 4 for each case study.

Table 4. Values of ϕ_i for each case study.

Case Study	Φ_1 [-]	Φ_2 [-]	Φ_3 [-]	Φ_4 [-]	Φ_5 [-]
1	0.206	0.402	0.608	0.788	1.00
2	0.262	0.519	1.00	-	-

The modal participation factor Γ is given by:

$$\Gamma = \frac{\sum_{k=1}^{n_s} m_k \phi_k}{\sum_{k=1}^{n_s} m_k \phi_k^2} \tag{15}$$

where the Γ and m_k values are reported in Table 5. While the dynamic parameters of the equivalent SDOF system are shown in Table 6 according to EN 1998-1-1 [32].

Table 5. Values of Γ and m_k for each case study.

Case Study	Γ [-]	m_1 [kg·10³]	m_2 [kg·10³]	m_3 [kg·10³]	m_4 [kg·10³]	m_5 [kg·10³]
1	1.364	60.346	60.346	60.346	60.346	60.346
2	1.331	54.234	54.234	54.234	-	-

Table 6. Dynamic parameters of the equivalent SDOF systems.

Case Study	m^* [kg·10³]	k^* [kN/m]	ω^* [rad/s]	T^* [s]
1	181.04	8668.21	6.920	0.91
2	96.63	1152.32	3.443	1.82

Therefore, the characteristic points of the capacity curve are defined in the planes $\alpha - \delta$, $F_b - d_c$, $F^* - D^*$, $S_a - S_D$ assessing the capacity in terms of accelerations for *Nassar and Krawinkler* approach and ADRS spectrum approach. The results based on the use of the ADRS spectrum and the *Nassar and Krawinkler* formulations are reported in Tables 7 and 8 for different structural levels [33–35]. In particular, the following results are indicated: α_{LS} is the multiplier of seismic forces for a specific limit state (LS); F_{LS} is base shear force corresponding to the specific LS; δ_{LS} is the maximum displacement of the top storey

corresponding to F_{LS}; F^* is the base shear force of the equivalent SDOF system; δ^* is the displacement of the equivalent SDOF corresponding to F^*; $S_a(T^*)$ is the spectral acceleration obtained by using the ADRS spectrum and for *Nassar and Krawinkler* approach.

Table 7. Capacity in terms of spectral acceleration and displacements according to ADRS Spectrum and Nassar and Krawinkler approach for the case study 1.

	MDOF			Equivalent SDOF		ADRS Spectrum	Nassar and Krawinkler
Limit State	α_{LS} [-]	δ_{LS} [m]	F_{LS} [kN]	δ^* [m]	F^* [kN]	$S_a(T^*)$ [g]	$S_a(T^*)$ [g]
Fully operational [FO]	2.27	0.086	742.99	0.063	544.86	**0.307**	**0.307**
Operational [O]	4.81	0.181	1572.21	0.133	1152.96	**0.649**	**0.649**
Life Safety [LS]	4.81	0.554	1572.21	0.406	1152.96	**1.983**	**2.040**
Near Collapse [NC]	4.66	0.858	1523.57	0.629	1117.28	**3.071**	**3.151**

Table 8. Capacity in terms of spectral acceleration and displacements according to ADRS Spectrum and Nassar and Krawinkler approach for the case study 2.

	MDOF			Equivalent SDOF		ADRS Spectrum	Nassar and Krawinkler
Limit State	α_{LS} [-]	δ_{LS} [m]	F_{LS} [kN]	δ^* [m]	F^* [kN]	$S_a(T^*)$ [g]	$S_a(T^*)$ [g]
Fully operational [FO]	0.42	0.096	115.48	0.072	86.77	**0.087**	**0.087**
Operational [O]	0.53	0.124	145.73	0.093	109.49	**0.112**	**0.112**
Life Safety [LS]	0.53	0.188	145.73	0.141	109.49	**0.171**	**0.182**
Near Collapse [NC]	0.40	0.245	109.98	0.184	82.63	**0.224**	**0.236**

5.2. Modelling in OpenSees

The numerical dynamic analyses have been performed through OpenSees (Python version 3.5.1) [37] (Supplementary Materials File S1).

Each tcl or Python file is characterised by a precise syntax, and the structural system model must follow the following order:

- **Geometric Data**: Defines the basic model and problem size for analysis, specifying the degrees of freedom for each node.
- **Nodal Coordinates:** Specifies the coordinates of all nodes in the x-y-z reference system, with the x-y plane as the working plane.
- **Constraints:** Establishes boundary conditions using the fix command for free or constrained degrees of freedom. Internal constraints, such as real hinges, are inserted using the EqualDof command.
- **Materials:** Defines the system's materials utilizing constitutive laws from the uniaxialMaterial library [37].
- **Sections:** Defines model sections using a fibre modelling approach, creating rectangular models with discretised fibres, often with specific commands like patch rect and wide flange.

- **Transformation:** Defines the transformation of the reference system to account for stiffness and stresses, such as a P-delta transformation for second-order effects in certain structural types.
- **Elements:** Defines individual elements of the system, associating end nodes, sections, and geometric transformations using default commands like *dispBeamColumn*, *nonLinearBeamColumn*, and *elasticBeam*.
- **Loads:** Specifies loads at nodes or previously defined elements. Often includes detailed steps on applying loads incrementally for nonlinear analysis, like the proportional application of gravitational loads in multiple steps.
- **Recorders:** Defines the outputs to be saved for analysis, commonly including element stresses and structural node displacements for data interpretation.
- **Analysis:** Sets up the solver for the system of equations, defines boundary conditions, numbering of equations, degrees of freedom, convergence tests, and algorithms used for solving nonlinear systems.

OpenSees allows performing a fibre modelling of the sections of the structural elements. It facilitates fibre modelling of structural element sections, allowing for nonlinear analyses by assigning constitutive properties to each fibre. This approach enables non-elastic behaviour within the materials, as each fibre represents a uniaxial behaviour. The structural element is divided into control sections, employing distributed plasticity, contrasting with concentrated plasticity, which focuses on plastic hinges.

Significant variations in element response occur based on the type of element modelling used, but the effective approximation of structural behaviour is achievable with proper mesh handling.

The fibre section is defined using the wide flange command, directly assigning the main section dimensions (Figure 12a). Elements are considered force-based.

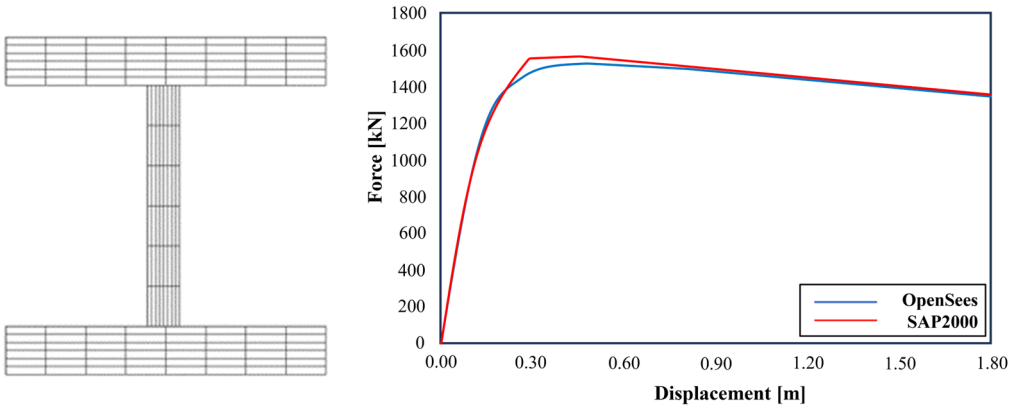

Figure 12. HEM 300 fibre section (**a**). Comparison between OpenSees and SAP2000 (**b**).

A 'Steel 02' Giuffrè–Menegotto–Pinto uniaxial material, representative of S355 steel grade, was utilised [38,39].

Figure 12b depicts the comparison between the static pushover curves obtained from SAP2000 and OpenSees for Case Study 1. Notably, the SAP2000 model employs lumped plasticity, utilizing P-Hinge properties. In contrast, Opensees replicates the structure's behaviour using distributed plasticity without incorporating any material hardening.

5.3. Definition of the Set Real Earthquakes

The structures, previously described, have been subjected to seven accelerograms, which have been opportunely chosen to assure that their average value was compatible with the design response spectra provided by the Italian seismic code [40] for soil type B and a PGA equal to 0.261 g.

The main features of the selected seven earthquakes are reported in Table 9, where the scaling factors are selected to let the average spectrum not exceed ±10% of the design spectrum (Figure 13).

Table 9. Selected set of earthquakes.

	Event ID	PGA [cm/s^2]	*Length* [s]	N_{pt} [-]	*ScaleFactor* [-]
S1	GR-1995-0047	510.615	6.18	7958	1.50
S7	IT-2009-0009	355.460	11.75	20000	1.28
S9	IT-1976-0030	341.508	4.795	4919	0.50
S13	IT-2009-0009	644.247	7.695	20001	0.75
S21	EMSC-20161030	476.428	10.395	10000	0.63
S25	IT-1980-0012	314.302	39.005	14152	0.80
S26	IT-1980-0012	58.702	35.200	10602	1.50

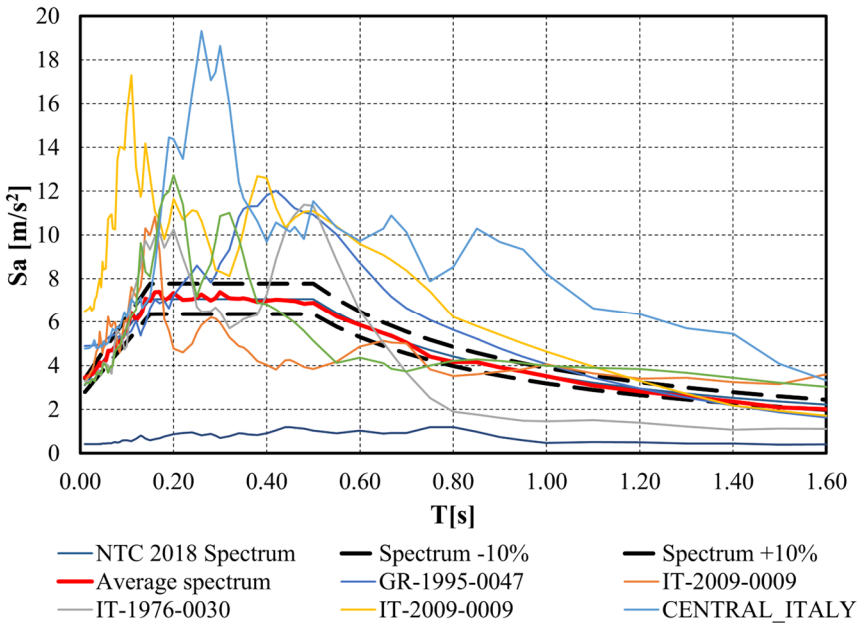

Figure 13. Selected accelerograms.

5.4. Results

The maximum inter-storey drift, i.e., the ratio between the maximum relative inter-storey displacement and the inter-storey height, has been evaluated as a function of the peak ground acceleration (PGA) for each earthquake and intensity level. The rotation capacity has been set according to EN 1998-1-3 [31], and the results are reported in Table 10 with reference to each case study and in accordance with the specific limit state.

The MIDR provides an estimate of the maximum rotation exhibited by the members (columns) of the structure. The corresponding S_a/g value was evaluated for each rotation as reported in Figure 14.

For each earthquake, the PGA/g corresponding to the achievement of the four limit states considered was derived, and the average value was determined. Given the average PGA/g, the corresponding spectral acceleration was derived by constructing a specific response spectrum in terms of accelerations.

Table 10. Rotation capacity according to EN 1998-1-3 [31].

Case Study	*Limit State*	*Rotation Capacity* θ_c
1	Damage Limitation [DL]	0.0078
	Significant Damage [SD]	0.047
	Near Collapse [NC]	0.063
2	Damage Limitation [DL]	0.0088
	Significant Damage [SD]	0.053
	Near Collapse [NC]	0.070

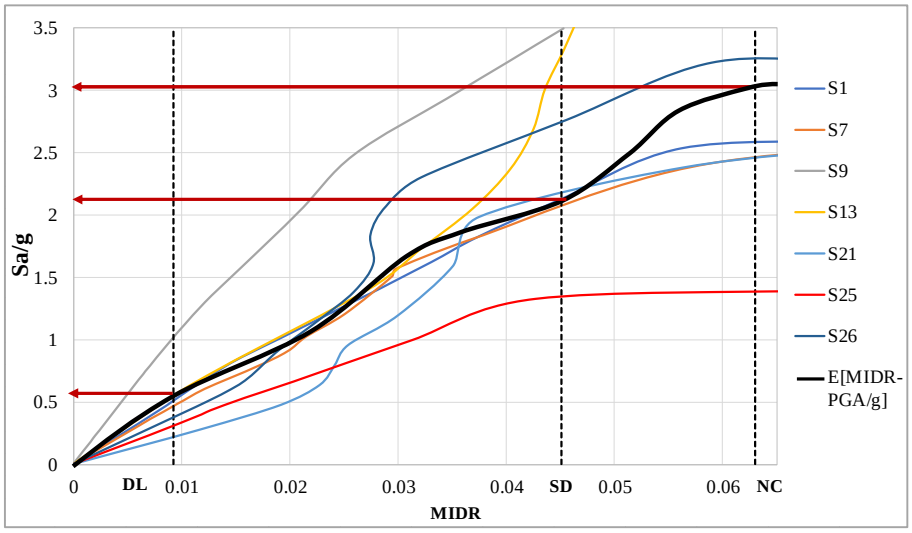

(**a**)

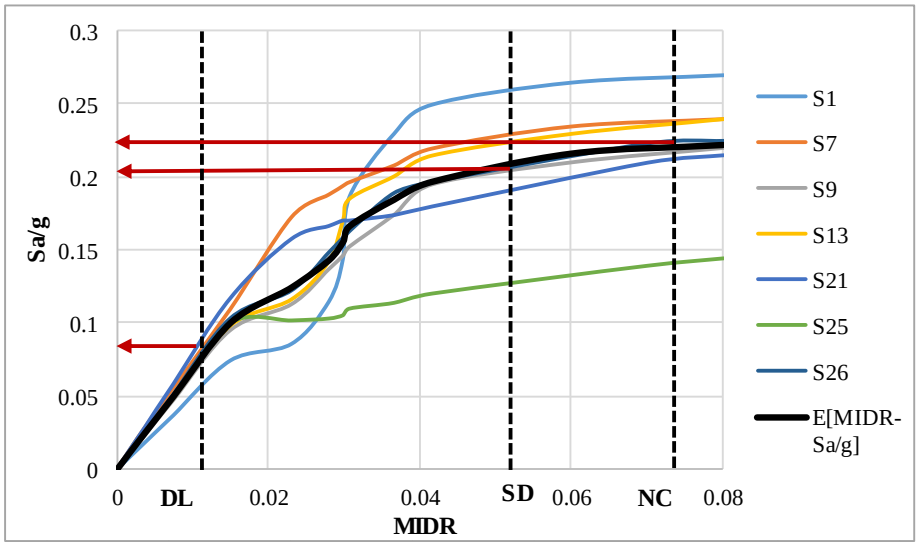

(**b**)

Figure 14. Sa/g value evaluated for each MIDR limit provided by EN1998-1-3 [31]: Case study 1 (**a**); Case study 2 (**b**).

The accelerations thus obtained were compared with those obtained through the application of the verification procedures described in the proposed simplified method, and the results are shown in Tables 11 and 12.

Table 11. Comparison between IDA results and Simplified Method in terms of spectral accelerations for case study 1.

Limit State	θ_c [rad]	$S_a(T^*)/g$		
		IDA	ADRS Spectrum	Nassar and Krawinkler
Fully operational [FO]—Point A	-	0.293	0.307	0.307
Operational [O]—Point B	0.0078	0.618	0.649	0.649
Life Safety [LS]—Point C	0.047	2.180	1.983	2.040
Near Collapse [NC]—Point D	0.063	3.010	3.071	3.151

Table 12. Comparison between IDA results and Simplified Method in terms of spectral accelerations for case study 2.

Limit State	θ_c [rad]	$S_a(T^*)/g$		
		IDA	ADRS spectrum	Nassar and Krawinkler
Fully operational [FO]—Point A	-	0.078	0.087	0.087
Operational [O]—Point B	0.009	0.0892	0.112	0.112
Life Safety [LS]—Point C	0.053	0.201	0.171	0.182
Near Collapse [NC]—Point D	0.070	0.230	0.224	0.236

In particular, for case study 1, i.e., Table 11, there is a percentage error in the evaluation of capacity in terms of spectral acceleration between the simplified approach and IDA equal to +4.50% for the "Fully Operational" limit state, −3.30% for the "Operational" limit state, −14.00% for the "Life Safety" limit state, and +2.00% for the "Near Collapse" limit state. The simplified method, in this case, underestimates the actual capacity of the MRF for the "Life Safety" limit state while slightly overestimating the one at the "Near Collapse" limit state.

In case study 2, i.e., Table 12, it can be observed that the percentage error in the evaluation of capacity in terms of spectral acceleration between the Simplified Method and IDA is equal to +10.30% for the "Fully Operational" limit state, +19.70% for the "Operational" limit state, −9.40% for the "Life Safety" limit state, and −2.50% for the "Near Collapse" limit state. In other words, the simplified method underestimates the capacity in terms of spectral acceleration for both the "Life Safety" and "Near Collapse" limits states resulting on the safe side.

6. Conclusions

The simplified performance-based approach herein applied and validated has the aim of assessing the seismic vulnerability of existing steel Moment Resisting Frames (MRFs) subjected to seismic actions. The proposed methodology consists of a trilinear approximation of the structural-behavioural curve, whose first branch is obtained through elastic analysis, while rigid-plastic analysis, considering second-order effects, helps define the second and third branches.

In this work, the validation of the method through pushover analysis and Incremental Dynamic Analysis (IDA), applied to a simulated design structure and a real building whose data are available in the literature, is carried out. The pushover analyses have been developed by the SAP2000 computer program. From the analysis of Figures 5 and 6, it is possible to notice the high levels of precision achieved, as evidenced by the mean value of the δ_{SAP}/δ_{th} ratios close to the unit and by the presence of points leaning against the trend line, which is very close to the bisector.

The IDAs were executed using the OpenSees software, employing a highly accurate fibre model that accurately reflects the behaviour of the analysed structures. This allowed for evaluating the actual percentage error between the seismic capacity defined by the simplified methodology and that obtained through the IDAs for each considered limit state.

The final part of the article is focused on the definition of the MIDR—Sa/g curves for each of the 7 earthquakes considered. The comparison in terms of spectral acceleration capacities between the simplified method and IDAs provided consistent results, with a maximum error of +2.00% for case study 1 and −2.50% for case study 2, both for the Near Collapse limit state.

Future developments may involve extending the methodology to medium- and high-rise buildings or to other structural types [41] to ensure an even wider applicability of the developed method.

Supplementary Materials: The following supporting information can be downloaded at: https://www.mdpi.com/article/10.3390/app14031037/s1.

Author Contributions: Conceptualization, V.P. and R.M.; Methodology, P.T. and R.M.; Software, P.T.; Validation, E.N., A.P. and P.T.; Formal analysis, P.T.; Investigation, E.N. and P.T.; Writing—original draft, A.P. and P.T.; Writing—review & editing, A.P. and P.T.; Supervision, V.P. and R.M. All authors have read and agreed to the published version of the manuscript.

Funding: This research received no external funding.

Institutional Review Board Statement: Not applicable.

Informed Consent Statement: Not applicable.

Data Availability Statement: The data presented in this study are available in Supplementary Materials.

Conflicts of Interest: The authors declare no conflict of interest.

References

1. Mazzolani, F.M.; Piluso, V. Plastic design of seismic steel frames. *Earthq. Eng. Struct. Dyn.* **1997**, *26*, 167–191. [CrossRef]
2. Piluso, V.; Pisapia, A.; Castaldo, C.; Nastri, E. Probabilistic theory of plastic mechanism control for steel moment resisting frames. *Struct. Saf.* **2019**, *76*, 95–177. [CrossRef]
3. Montuori, R.; Nastri, E.; Piluso, V.; Pisapia, A. Design procedure for failure mode control of linked column frames. *Eng. Struct.* **2023**, *296*, 116937. [CrossRef]
4. Suzuki, A.; Iervolino, I. Seismic Fragility of Code-conforming Italian Buildings Based on SDoF Approximation. *J. Earthq. Eng.* **2021**, *25*, 2873–2907. [CrossRef]
5. Yamada, S.; Miyazawa, H.; Iyama, J. Seismic performance of weak-beam-type steel low-to-middle-rise moment-resisting frame determined by local buckling of square hollow section columns. *Thin-Walled Struct.* **2024**, *195*, 111359. [CrossRef]
6. Hou, J.; Lu, J.; Chen, S.; Li, N. Study of seismic vulnerability of steel frame structures on soft ground considering group effect. *Structures* **2023**, *56*, 104934. [CrossRef]
7. Ruggieri, S.; Chatzidaki, A.; Vamvatsikos, D.; Uva, G. Reduced-order models for the seismic assessment of plan-irregular low-rise frame buildings. *Earthq. Eng. Struct. Dyn.* **2022**, *51*, 3327–3346. [CrossRef]
8. van der Burg, L.; Kohrangi, M.; Vamvatsikos, D.; Bazzurro, P. A risk-based evaluation of direct displacement-based design. *Bull. Earthq. Eng.* **2022**, *20*, 6611–6633. [CrossRef]
9. Tsarpalis, D.; Vamvatsikos, D.; Vayas, I. Seismic assessment approaches for mass-dominant sliding contents: The case of storage racks. *Earthq. Eng. Struct. Dyn.* **2022**, *51*, 812–831. [CrossRef]
10. Liguori, F.S.; Madeo, A.; Formisano, A. Seismic vulnerability of industrial steel structures with masonry infills using a numerical approach. *Bull. Earthq. Eng.* **2023**. [CrossRef]

11. Landolfo, R.; Formisano, A.; Di Lorenzo, G.; Di Filippo, A. Classification of European building stock in technological and typological classes. *J. Build. Eng.* **2022**, *45*, 103482. [CrossRef]
12. Silva, A.; Macedo, L.; Monteiro, R.; Castro, J.M. Earthquake-induced loss assessment of steel buildings designed to Eurocode 8. *Eng. Struct.* **2020**, *208*, 110244. [CrossRef]
13. Cheng, S.; He, H.; Sun, H.; Cheng, Y. Rapid recovery strategy for seismic performance of seismic-damaged structures considering imperfect repair and seismic resilience. *J. Build. Eng.* **2024**, *82*, 108422. [CrossRef]
14. Hickey, J.; Broderick, B. Loss impact factors for lifetime seismic loss assessment of steel concentrically braced frames designed to EC8. *J. Struct. Int. Maint.* **2019**, *4*, 110–122. [CrossRef]
15. Yang, K.; Tan, P.; Chen, H.; Li, J.; Tan, J. Prediction of nonlinear seismic demand of inter-story isolated systems using improved multi-modal pushover analysis procedures. *J. Build. Eng.* **2024**, *82*, 108322. [CrossRef]
16. Prota, A.; Tartaglia, R.; Di Lorenzo, G.; Landolfo, R. Seismic strengthening of isolated RC framed structures through orthogonal steel exoskeleton: Bidirectional non-linear analyses. *Eng. Struct.* **2024**, *302*, 117496. [CrossRef]
17. Mohammadgholipour, A.; Billah, A.M. Performance-based plastic design and seismic fragility assessment for chevron braced steel frames considering aftershock effects. *Soil Dyn. Earthq. Eng.* **2024**, *178*, 108440. [CrossRef]
18. Macedo, L.; Castro, J.M. Collapse performance assessment of steel moment frames designed to Eurocode 8. *Eng. Fail. Anal.* **2020**, *126*, 105445. [CrossRef]
19. Montuori, R.; Nastri, E.; Piluso, V. Theory of plastic mechanism control: A new approach for the optimization of seismic resistant steel frames. *Earthq. Eng. Struct. Dyn.* **2022**, *51*, 3598–3619. [CrossRef]
20. Kalapodis, N.A.; Muho, E.V.; Qian, J.; Zhou, Y. Assessment of seismic inelastic displacement profiles of steel MRFs by means of modal behavior factors. *Soil Dyn. Earthq. Eng.* **2023**, *175*, 108218. [CrossRef]
21. Kim, J.; Sause, R. Design concepts for avoiding story mechanism in steel MRFs under seismic loading. *Earthq. Eng. Struct. Dyn.* **2023**, *52*, 750–775. [CrossRef]
22. Huang, Z.; Cai, L.; Pandey, Y.; Tao, Y.; Telone, W. Hysteresis effect on earthquake risk assessment of moment resisting frame structures. *Eng. Struct.* **2021**, *242*, 112532. [CrossRef]
23. Maddah, M.M.; Eshghi, S.; Garakaninezhad, A. A new optimized performance-based methodology for seismic collapse capacity assessment of moment resisting frames. *Struct. Eng. Mech.* **2022**, *82*, 667–678.
24. Baltzopoulos, G.; Grella, A.; Iervolino, I. Seismic reliability implied by behavior-factor-based design. *Earthq. Eng. Struct. Dyn.* **2021**, *50*, 4076–4096. [CrossRef]
25. Petruzzelli, F.; Iervolino, I. NODE: A large-scale seismic risk prioritization tool for Italy based on nominal structural performance. *Bull. Earthq. Eng.* **2021**, *19*, 2763–2796. [CrossRef]
26. El Jisir, H.; Kohrangi, M.; Lignos, D.G. Proposed nonlinear macro-model for seismic risk assessment of composite-steel moment resisting frames. *Earthq. Eng. Struct. Dyn.* **2022**, *51*, 1180–1200. [CrossRef]
27. Montuori, R.; Nastri, E.; Piluso, V.; Todisco, P. A simplified performance based approach for the evaluation of seismic performances of steel frames. *Eng. Struct.* **2020**, *224*, 111222. [CrossRef]
28. Montuori, R.; Nastri, E.; Piluso, V.; Todisco, P. Evaluation of the seismic capacity of existing moment resisting frames by a simplified approach: Examples and numerical application. *Appl. Sci.* **2021**, *11*, 2594. [CrossRef]
29. Montuori, R.; Nastri, E.; Piluso, V.; Todisco, P. Simplified approach for the seismic assessment of Existing X shaped CBFs: Example and numerical applications. *J. Comp. Sci.* **2022**, *6*, 62. [CrossRef]
30. Montuori, R.; Nastri, E.; Piluso, V.; Todisco, P. Performance-based rules for the simplified assessment of steel CBFs. *J. Constr. Steel Res.* **2022**, *191*, 107167. [CrossRef]
31. *EN 1998-1-3*; Design of Structures for Earthquake Resistance—Part 3: Assessment and Retrofitting of Buildings. European Committee for Standardization (CEN): Brussels, Belgium, 2004.
32. *EN 1998-1-1*; Design of Structures for Earthquake Resistance—Part 1: General Rules, Seismic Actions and Rules for Buildings. European Committee for Standardization (CEN): Brussels, Belgium, 2004.
33. *SAP2000*, version 24; Structural and Earthquake Engineering Software; Computer & Structures, Inc.: Berkeley, CA, USA, 2024. Available online: https://www.csi-italia.eu/(accessed on 22 January 2024).
34. Nassar, A.A.; Krawinkler, H. *Seismic Demands for SDOF and MDOF Systems*; Technical Report 95; John A. Blume Earthquake Engineering Center, Stanford Digital Repository: Stanford, CA, USA, 1991.
35. Gupta, A.; Krawinkler, H. *Seismic Demands for Performance Evaluation of Steel Moment Resisting Frames Structures*; Technical Report 132; John A. Blume Earthquake Engineering Center, Stanford Digital Repository: Stanford, CA, USA, 1999.
36. Fajfar, P. A nonlinear analysis method for performance-based seismic design. *Earthq. Spec.* **2000**, *16*, 573–592. [CrossRef]
37. Open System for Earthquake Engineering Simulation (OpenSees). *Pacific Earthquake Engineering Research Centre*; University of Berkeley: Berkeley, CA, USA, 1999; Available online: https://opensees.berkeley.edu/ (accessed on 22 January 2024).
38. Filippou, F.C.; Popov, E.P.; Bertero, V.V. *Effects of Bond Deterioration on Hysteretic Behavior of Reinforced Concrete Joints*; Report EERC 83-19; Earthquake Engineering Research Center, University of California: Berkeley, CA, USA, 1983.
39. Nguyen, V.T.; Nguyen, X.D. Optimal Procedure for Determining Constitutive Parameters of Giuffrè–Menegotto–Pinto Model for Steel Based on Experimental Results. *Int. J. Steel Struct.* **2022**, *22*, 851–863. [CrossRef]

40. European Commission. *DM 17.01.2018: New Technical Code for Constructions*; Ministry of Infrastructures and Transports: Rome, Italy, 2018.
41. Meng, B.; Xiong, Y.; Zhong, W.; Duan, S.; Li, H. Progressive collapse behaviour of composite substructure with large rectangular beam-web openings. *Eng. Struct.* **2023**, *295*, 116861. [CrossRef]